Laser welding of aluminium alloys 5083 and 6082 under conduction regime.

J.M. Sánchez-Amaya, T. Delgado, L. González-Rovira, F.J. Botana.

Departamento de Ciencia de Materiales e Ingeniería Metalúrgica y Química Inorgánica. Grupo de Ensayos, Corrosión y Protección. Universidad de Cádiz. Lab. 712, CASEM. Avda. República Saharaui s/n, 11510 Puerto Real, Cádiz. Spain.

Abstract

In this work, samples of aluminium alloys 5083-T0 and 6082-T6 have been welded under conduction regime, using a High Power Diode Laser. The influence of experimental variables, as the laser power and the linear welding rate, on the sizes and properties of the butt weld beads has been studied. In addition to measure the depths and widths of the weld beads, their microstructure, microhardness profile and corrosion resistance have been analysed. The results obtained allow one to define the experimental conditions leading to good quality butt welds with higher penetration than those published in the recent literature. Maximum penetration values of 3 mm and 2.3 mm were obtained for 5083 and 6082, respectively. Additionally, a simple mathematical expression relating the weld depth (d) with the laser power (P) and the processing rate (v) has been proposed: $d = \frac{P - b \cdot b'}{a \cdot v} - \frac{b \cdot a'}{a}$, being a, a', b and b' constant values for each alloy. This equation shows a good fitting to the experimental depth values, proving its ability to predict the penetration of 5083 and 6082 welds generated under conduction regime.

Keywords:

Laser welding, aluminium alloys, conduction regime, depth estimation, corrosion resistance.

1. Introduction.

The laser welding is a promising technology to a lot of industrial sectors because of the possibility of joining and repairing different materials. Laser welding technology have some disadvantages in comparison with other conventional joining technologies, as the high costs of equipment, strict requirements concerning the laser beam adjustment and the samples alignment. However, laser welding show important advantages compared with other techniques, as the low heat input, the high localization ability, the high welding speed, the high flexibility, the high weld quality and the high production rate [1-5].

It is reported elsewhere [1,2,6] that laser welding can be carried out by means of two different regimes: keyhole and conduction. Keyhole regime involves the employment of higher density power and usually leads to narrower welding beads than the conduction regime [4,5,7,8]. The former mechanism often generates welding beads with high porosity due to gas entrapment occurring during the solidification of the weld pool. In contrast, conduction welding is a more stable process because the metal evaporation takes place at a lower level than at keyhole mode [1,2]. In fact, it has been recently reported that aluminium alloy 5083 has magnesium lost of about 1-4% when welded under conduction mode [1], while 13-22% under keyhole regime [9].

The laser welding is generally more difficult to apply to aluminium alloys [10,11] than to steel alloys, due to its higher reflectivity, higher thermal conductivity and lower viscosity [5,12]. Thus, the thermal conductivity of aluminium alloys (143 $W\ m^{-1}\ K^{-1}$) is about one order of magnitude higher than that of steels (14 $W\ m^{-1}\ K^{-1}$) [1,13]. Additionally, aluminium alloys have high reflectivity (sometimes higher than 80%), being more reflective as the aluminium alloy is purer. The high reflectivity makes the aluminium alloys absorb low fraction of the incident radiation; the high thermal conductivity provokes a rapid heat transfer, avoiding the concentration of energy in the weld pool; and finally, the lower viscosity of the welding pool limits the expansion of the pool before the solidification [1].

Little research has been reported on welding 5XXX and 6XXX aluminium alloys under conduction regime with diode laser [1,14]. Among them, in [14] a high

power diode laser has been successfully employed to weld 5022 and 6016 aluminium alloys. In this paper, samples of 1 mm thickness were successfully welded, being analysed the influence of the processing rate on the depths and widths of the welds obtained. It was observed that at 4 KV, full penetration bead-on-plate and butt welding was achieved up to a welding speed of 12 m/min for 5022 and 6 m/min for 6016 [14]. The maximum welding speed to get full penetration varies in these alloys due to their different heat conductivity. In [1], bead-on-plate welds of 5083 samples free of defects were obtained at 1.5 or 3 m/min and 1.5 KV, analysing the influence of the superficial treatment and the processing rate on the welds properties. The penetration under these conditions ranged between 0.4 and 0.9 mm. In addition to measure the width and the depths, the microstructure, the microhardness and the corrosion resistance of the different zones of the beads were studied [1].

The main objective of the present paper is to widen the knowledge related to welding aluminium alloys under conduction mode with diode laser. 5083 and 6082 aluminium alloy samples have been processed with a High Power Diode Laser of a maximum power of 2.8 KW in order to generate butt welds of higher penetration than those published in the recent literature (1 mm) [1,14]. The size and properties of the welds obtained with different laser powers (between 1.5 and 2.75 KW) and processing rates (between 0.2 and 5 m/min) have been studied. Additionally, a simple analytical expression has been proposed to predict the bead depths in function of the alloy, the laser power and the welding rate.

2. Experimental.

The chemical composition of the aluminium alloys 5083-T0 and 6082-T6 employed in this study are given in Table 1. Sheets of these alloys, whose thicknesses were 3 mm in the case of the 5083 and 4 mm in the case of 6082, were cut to obtain samples of 70 long and 14 mm wide. Before welding, these work pieces were sandblasted with white corindon particles. This superficial treatment involves a notable increase of radiation absorption, as it reduces the reflectivity level of the surface. Other methods can be used to increase the energy absorption, as the application of black coatings. However, it has been recently proved that the sandblasting treatment provides

a better corrosion resistance than other treatment of increasing the laser absorption, since the magnesium evaporation is minimised [1]. After sandblasting, the welding edges of samples were polished using 320grit SiC paper to get an efficient physical join between them. The surface was later degreased with acetone and subjected to the laser treatments. All treatments and measurements have been made in triplicate to assure the reproducibility.

Butt welding was performed on the aluminium alloys samples using a High Power Diode Laser with a maximum power of 2.8 KW. The parameters of the laser beam employed to generate butt welds under conduction regime are included in Table 2. All the laser treatments were carried out in continuous mode and the focal position was situated at the specimen surface to obtain the higher power density.

The influence of the welding rate and the laser power on the characteristics of weld beads has been studied. The values of power employed were between 1.5 KW and 2.75 KW, the laser processing rates were between 0.2 m/min and 5 m/min, and the added shielding gas was Nitrogen with a flow rate of 15 Nl/min. It is widely known that the shielding gas plays a very important role in welding aluminium alloys, preventing the oxide formation that could affect the metallurgical properties of welds [5,11].

The microstructure of the generated welds was analysed by optical microscopy. Thus, metallographic images of the weld beads cross-sections were studied. To perform this analysis, the welded samples were cut, mounted, polished and etched with Keller for 5 seconds. The depth and width were measured for each experimental condition. Vickers microhardness measurements were also carried out on transversal sections of welding beads following the standard ASTM E 384 [15]. The charge employed was 490,3 mN during 19 seconds. Microhardness maps and profiles of representative welds have been measured. Finally, the corrosion behaviour of welded samples was studied. These samples were immersed in NaCl + H_2O_2 solution at 30ºC for 6 hours, following the standard test ASTM G 110 [16]. After this exposure, the cross-sections of the welds were analysed metallographically.

3. Results and discussion.

Butt welds were generated on 5083 and 6082 samples under conduction regime using a high power diode laser, employing different welding rates and laser powers. In continuation, the morphology and size of the beads are reported. Additionally, an analytical equation has been proposed to predict the penetration in function of the laser power and the processing rate. Finally, the microstructure, the mechanical and corrosion properties of the welds are analysed.

3.1. Morphology and size of the welding beads.

Firstly, the results obtained from the metallographic study of the butt weld beads are presented. Metallographic images of butt weld beads cross-sections of 5083 and 6082 samples are included in Figure 1 and 2, respectively. In these figures, it can be observed that in all conditions the shape of the formed butt welds tends to be a semicircle in which the relation between depth and width has an approximated value of 0.5. This characteristic morphology confirms that the weld beads are generated under conduction regime. As can be seen in the metallographic images, this regime [1] leads to beads with much lower porosity than the weld beads that are usually obtained under keyhole regime [2,5]. It can be observed in Figures 1 and 2 that some 5083 welds only show small porous in the lower part of the weld bead. This low porosity appears as a consequence of the gas entrapment during the bead solidification. It was observed that the weld beads of the alloy 6082 do not show any sign of porosity. However, the beads of this latter alloy present cracks along the welding beads. These cracks are thought to be due to the tensions formed during the solidification. As can be appreciated in Figure 2, the extension of the cracks diminishes as the laser power is increased and the welding rate is decreased.

It could be checked that when the power was low and the welding rate was high, the samples were not totally welded, that is, the welding efficiency was not 100%. In Figure 3, two examples of partially (a) and totally (b) welded samples can be seen. The welding efficiency in terms of percentage has been measured for all conditions studied, and have been plotted in Figure 4. According to the data included in this figure, when the laser power is 2.5 KW, 5083 samples are fully welded at a processing rate equal or

below 4.5 m/min, while 6082 samples are totally joint only when the rate is equal or below 1 m/min.

As expected [1], it is apparent from the images of Figure 1 and 2, that the bead sizes are higher as the laser power is increased and/or the welding rate is decreased. The depth and width measurements of the 5083 butt weld beads are presented in Figures 5 and 6, respectively. Meanwhile the values of these parameters for the 6082 alloy are also included in Figures 7 and 8, respectively. If the depth and the width values of these figures are compared, it can be seen that under similar conditions, both parameters are generally higher for 5083 than for 6082. This means that for a given laser power and welding rate, the butt welding bead generated on 5083 is higher than the one formed on 6082. Therefore, to get similar penetration values in both alloys, it is necessary to employ more energetic conditions when welding 6082 samples.

When the influence of both the laser power and the welding rate on the bead size are analysed in Figures 5 to 8, one can appreciate that the welding rate influence more strongly than the laser power. Indeed, the bead dimensions show a higher variation when the welding rate is modified than when it is the laser power. Therefore, in conduction mode, the effect of power level applied over the samples is not so marked as the processing rate. However, both variables determine the final characteristics of the butt welding bead.

In Figure 9, the values of the product "*Depth*Width*" for both alloys in function of the welding rate are represented (in double logarithmic scale). It can be seen in this figure that the size tendency is similar for both alloys. Additionally, it can be easily observed that, in general terms, the butt welding beads of 5083 samples have higher size than those of 6082 samples. Concisely, under similar experimental conditions the penetration values of the butt welding beads of 5083 samples are around 40% higher than the beads of 6082 samples. For example, the penetration depth at 2 KW and 0.5m/min is 1.62 mm for 5083 and 1.11 mm for 6082. This feature is thought to be due to the different thermal properties of both alloys. Thus, at room temperature, the thermal conductivity of the alloy 5083 can range between 105 and 120 W/m·K, while the value of this parameter for 6082 can be between 150 and 170 W/m·K, approximately a 40% higher than the value for 5083 [17]. This difference is probably due to the different

amount of alloying elements of both alloys [17]. Thus, the total percentage of alloying elements is 5.27% in 5083 and 2.96% in 6082. As the thermal conductivity is lower in 5083 than in 6082, in the former alloy the heat is more concentrated in the fusion pool during the laser welding and consequently the energy is less transferred to the surrounding areas. This implies that under similar experimental conditions of laser power and processing rate, 5083 samples can keep a higher energy in the fusion pool than 6082 samples. Therefore, similar input energy produces bigger size of welding bead in 5083 than in 6082 samples. In short, as 5083 has higher percentage of alloying elements than 6082, it has lower thermal conductivity, that leads to welding beads of higher sizes.

3.2. Analytical estimation of weld depth.

Some empirical data regarding the relationship between the laser power (P), the welding speed (v) and the bead depth (d) and width (w) can be found in the literature in the case of the laser welding of different alloys under keyhole regime [6]. Although different relationships are proposed, some features are common to all these experimental results: an increase in the laser power or a decrease in the welding speed lead to an increase of the bead depth and width. According to [6], the analytical expression fitting these data is the following:

$$\frac{P}{v \cdot d} = a + \frac{b}{w} \tag{1}$$

where P (KW) is the laser power; v (mm/sec), the welding speed; w (mm), the width; and d (mm), the depth of the welding bead. Similarly, a and b are the constant values obtained from these fits, which strongly depend on the laser source. Thus, the welding of aluminium alloys with a CO_2 laser and a Nd:YAG laser give the values of a, b and R^2 reported in Table 3 [6]. One has to take into account that these estimations have been obtained under keyhole regime, which is not our case, as in this work the samples were welded under conduction regime. Figures 10 and 11 show the fitting obtained in the present work for the 5083 and 6082 alloys, respectively. The first noticeable feature that can be seen in these figures is that the slope b is negative, in contrast to values previously reported in [6]. Such difference could stem from the kind of regime used to

weld the samples. Therefore, it seems that *b* is negative under conduction regime and positive under keyhole regime. Additionally, it can be seen in this figure that fitting of the equation to 5083 data is better than to 6082 data. Besides, the slope (*b*) of the fitting line of the 5083 alloy is smaller than that corresponding to 6082.

Rearranging equation (1), it is possible to obtain equation (2), which allows an estimation of *d* from *P*, *v* and *d/w* values.

$$d = \frac{P}{a \cdot v} - \frac{d \cdot b}{a \cdot w} \tag{2}$$

These *P* and *v* values in equation (2) are experimentally fixed, and consequently, can be directly fed into this expression. However, in order to estimate the penetration as a function of *P* and *v*, it is necessary first to estimate an expression relating *d/w* with *P* and *v* from our experimental data. Figures 12 and 13 depict the *d/w* values obtained for both 5083 and 6082 alloys, as a function of *P* and v^{-1}. Only those data corresponding to totally welded samples have been considered. As easily seen in these figures, the whole set of data can be fitted to a line, whose ordinate at the origin and slope values are *a'* and *b'* correspondingly:

$$d / w = a' + \frac{b'}{v} \tag{3}$$

The values of *a'* and *b'* of the fitting lines, as a function of the alloy and the laser power are presented in Table 4. From Figures 12 and 13 and this table, it can be observed that the values of *a'* are quite similar for both alloys, between 0.28 and 0.3, independently of the laser power employed. The values of *b'* also seem to be independent of the laser power, but they are different for each alloy (between 0.74 and 1.17 mm·sec^{-1} for 5083 and between 0.45 and 0.54 mm·sec^{-1} for 6082). Therefore, it seems that the laser power does not influence the *d/w* values, the processing rate being the main parameter affecting the *d/w* value. Therefore, *a'* and *b'* can be proposed as characteristic values for each alloy. The average values of *a'* are 0.2970 for 5083 and 0.2953 for 6082, whereas average values of *b'* were 1.0076 mm·sec^{-1} for 5083 and 0.5059 mm·sec^{-1} for 6082. Consequently, it can be stated that the representative values

of *a'* and *b'* are those included in Table 4: *a'*=0.3 for both alloys; and *b'* =1 mm·sec^{-1} for 5083 and *b'* =0.5 mm·sec^{-1} for 6082.

Combining the equations (2) and (3), it can be obtained the equation (4), an analytical expression of the weld penetration, *d*, in function of simple experimental variables, *P* and *v*, and four constants, *a*, *b*, *a'* and *b'*, whose values are provided in Tables 3 and 4.

$$d = \frac{P - b \cdot b'}{a \cdot v} - \frac{b \cdot a'}{a} \tag{4}$$

Thus, from equation (4), it is possible to estimate the penetration depth (in mm) for both 5083 (equation 5) and 6082 (equation 6) alloys:

$$d = \frac{P + 0.647}{0.3043 \cdot v} + 0.63786 \tag{5}$$

$$d = \frac{P + 0.358}{0.4900 \cdot v} + 0.43837 \tag{6}$$

In Figures 14 and 15, the real penetration values are compared with the values obtained from the simulation (equation 4). As can be appreciated, the simulated values are quite similar to the real ones, proving the validity of the proposed analytical expression.

3.3. Microstructure of the welding beads.

It has been observed that the microstructure of the different beads is similar for both alloys and for all the studied conditions. The main difference found when modified the laser power and the processing rates are the values of width and depth of the fusion zone. In Figure 16, cross-section micrographs of the butt weld bead formed when 5083 was processed at *P*=2KW and *v*=1 m/min have been included. In this figure, the typical microstructure of the welding beads obtained under the previously working conditions can be observed. Figure 16 (B) shows an image of the interface base metal/fusion zone

of the same bead. The microstructure of the base metal, Figure 16 (C), is very different from that of the Fusion Zone. As previously reported in [1], the external zones of the bead close to the base metal, Figure 16 (D), are characterised by showing a dendritic growth, which correspond to the zones with higher solidification rates. Additionally, it can be seen that the microstructure of the inner part of the Fusion Zone consists of a fine precipitation of the second phases in a solid solution matrix of aluminium, as shows Figure 16(E).

3.4. Microhardness test of the welding beads.

Microhardness tests were performed in order to characterize the weld affected area, including fusion zone (external and internal part) and the base metal surrounding the bead. The microhardness values were measured on a cross-section according to [15], following the scheme of Figure 17 (A). In order to compare the values obtained for both alloys studied, two conditions leading to welding beads of similar depth (1.2 mm) have been chosen for each alloy: P=2.5KV, v=0.5m/min for 5083 and P=2.5KV, v=1m/min for 6082. The Vickers microhardness values obtained for both 5083 and 6082 beads have been included in Figures 17 (B) and (C), respectively. As can be observed, in both alloys the microhardness values of the fusion zone are slightly higher (between 5 and 10 HV) than the values of the base metal surrounding the bead. These results agree with those reported in [1]. The little microhardness differences between the fusion zone and the surrounding base metal are related to the microstructural changes described above (in the section 3.3) [1,18].

The microhardness values have been also measured in different zones of the base metal. For this purpose, the indentations were performed on cross-sections of the beads, in a line parallel to the surface. The Figure 18 shows the microhardness profiles for both alloys. The microhardness values of both alloys (base metal not treated with laser) have been also included in the figure as references. In this figure, it can be seen that 5083 bead values do not change significantly with the distance to the fusion zone. The reference value of the base metal is also similar to the butt weld bead values. However, the values of the 6082 weld bead are much lowers than that of the base metal, indicating that the hardness provided by the original heat treatment of this alloy (T6) is reduced as a consequence of the laser treatment. In addition, it can be appreciated in

Figure 18 that the microhardness profile of 6082 reaches a minimum at 7 mm from the centre of the fusion zone, the values being recovered further this distance.

3.5. Corrosion test of the welding beads.

It was observed that, in general terms, 5083 and 6082 welds showed a good corrosion resistance, provided the high aggressiveness of the testing solutions. In fact, the fusion zone of the welds does not show corrosion as shown in Figure 19. However, some signs of localized corrosion could be seen at the zones surrounding the weld beads when the laser processing rate is low (Figure 20). Additionally, it could be observed in both alloys a low depth intergranular corrosion (IGC) in the base metal, as shows Figure 21. This feature is thought to be related to the microhardness decrease observed in the profile of Figure 18, which leads to a higher corrosion sensibilization. These attacks seem to appear at higher distances from the welding beads in 5083 samples than in 6082 samples. In 6082 samples, this IGC seems to be reduced when the processing rate is equal or higher than 0.3 m/min.

To sum up, the analyses of the samples after the corrosion tests revealed the occurrence of two different corrosion mechanisms. The first one consists of a localized corrosion attack at the boundary between the fusion zone and the base metal, and the second one, an intergranular corrosion attack taking place at the base metal out of the fusion zone. It was observed that the intensity of both types of corrosion increases as the welding rate decreases. Although these types of localised corrosion have been detected in the welded samples after the tests, it can be stated that the weld beads show, in general terms, a good corrosion resistance, as the solutions employed in the corrosion tests are known to be very aggressive [19].

4. Conclusions.

In this work, aluminium alloys 5083 and 6082 are welded under conduction regime with High Power Diode Laser. The influence of the laser power and the processing rate on the butt weld size is analysed. Although both variables determine the final size of the welding beads, it is appreciated that the welding rate influence more strongly than the laser power.

Butt welds with higher penetration than those published in the recent literature (1 mm) are obtained, reaching depth values up to 3.0 mm (full penetration) in 5083 samples and values up to 2.3 mm in the case of 6082. Under similar experimental conditions, the penetration values of 5083 beads are around 40% higher than the 6082 beads. This different behaviour of these alloys is related to the thermal properties, which depend on the total amount of alloying elements.

After studying the depths of the weld beads, a simple mathematical expression relating the weld depth with the laser power and the processing rate is proposed. The obtained analytical equation is proved to estimate accurately the butt weld depths of the studied alloys. Therefore, this expression can be used to predict, before performing the laser treatments, the weld penetration of both 5083 and 6082 alloys under conduction regime.

Finally, the microstructure, microhardness and corrosion resistance of the weld beads were studied. The microstructure of the different beads is similar for both alloys and for all the studied conditions. The fusion zone has two zones, an external zone showing a dendritic growth, and an inner part with a fine precipitation of the second phases in a solid solution matrix of aluminium.

Concerning the bead properties, it is observed that in both alloys, the microhardness of the fusion zone is slightly higher than that of the base metal surrounding the bead. The corrosion results show that low penetrating localised attacks are detected in the welded samples after the tests. However, taking into account the high aggressiveness of the testing solutions, it can be stated that the weld beads show, in general terms, a good corrosion resistance.

5. Acknowledgements.

The present work has been financially supported by the Ministerio de Educación y Ciencia (projects DPI2005-09244-C04-02 and MAT2008-06882-C04-02/MAT) and by the Junta de Andalucía.

6. References.

[1] J. M. Sánchez-Amaya,T. Delgado, J. J. De Damborenea, V. Lopez and F. J. Botana. "Laser welding of AA 5083 samples by high power diode laser". *Science and Technology of Welding and Joining*, Vol.14 (1), (2009) 78-86.

[2] P. Okon, G. Dearden, K. Watkins, M. Sharp, P. French. "Laser Welding of Aluminium Alloy 5083". *21st International Congress on Applications of Lasers and Electro-Optics*, Scottsdale, October 14-17, 2002 (ICALEO 2002) ISBN 0-912035-72-2.

[3] R.G. Ding, O.A. Ojo, M.C. Chaturvedi. "Laser beam weld-metal microstructure in an yttrium modified directionally solidified Ni3Al-base alloy" *Intermetallics* 15 (2007) 1504-1510.

[4] R. Akhter, L. Ivanchev and H.P. Burger "Effect of pre/post T6 heat treatment on the mechanical properties of laser welded SSM cast A356 aluminium alloy". *Materials Science and Engineering: A*, Vol 447 (2007) 192-196.

[5] T.Y. Kuo and H.C. Lin "Effects of pulse level of Nd-YAG laser on tensile properties and formability of laser weldments in automotive aluminum alloys" *Materials Science and Engineering: A*, Vol 416 (2006) 281-289.

[6] W.W. Duley, Laser Welding, New York, John Wiley and Sons, Inc., 1998: Chapter 4.

[7] Y. Shi, F. Zhonga, X. Li, S. Gong, L. Chen. "Effect of laser beam welding on tear toughness of a 1420 aluminum alloy thin sheet". *Materials Science and Engineering A* 465 (2007) 153–159.

[8] P. Bassani, E. Capello, D. Colombo, B. Previtali, M. Vedani. "Effect of process parameters on bead properties of A359/SiC MMCs welded by laser" *Composites: Part A* 38 (2007) 1089–1098.

[9] T. Sibillano, A. Ancona, V. Berardi, E. Schingaro, P. Parente and P.M. Lugarà. "Correlation spectroscopy as a tool for detecting losses of ligand elements in laser welding of aluminium alloys". *Optics and Lasers in Engineering* 44 (2006) 1324–1335.

[10] J. Yan, X. Zeng, M. Gao, J. Lai and T. Lin. "Effect of welding wires on microstructure and mechanical properties of 2A12 aluminum alloy in CO2 laser-MIG hybrid welding". *Applied Surface Science,* Vol. 255, Issue 16 (2009) 7307-7313.

[11] G. Campana, A. Ascari, A. Fortunato, G. Tani. "Hybrid laser-MIG welding of aluminum alloys: The influence of shielding gases". *Applied Surface Science*, Vol. 255, Issue 10 (2009) 5588-5590.

[12] N. Pierron, P. Sallamand, S. Matteï. "Study of magnesium and aluminium alloys absorption coefficient during Nd:YAG laser interaction". *Applied Surface Science*, Vol. 253, Issue 6 (2007) 3208-3214.

[13] H. Ahmed, M.A. Wells, D.M. Maijer, B.J. Howes and M.R. van der Winden. "Modelling of microstructure evolution during hot rolling of AA5083 using an

internal state variable approach integrated into an FE model" *Materials Science and Engineering A* .Vol. 390, Issues 1-2 (2005) 278-290

[14] N. Abe, M. Tsukamoto, K. Maeda, K. Namba and J. Morimoto. "Aluminum alloy welding by using a high power direct diode laser". *Journal of laser applications*. Vol 18 (4) (2006) 289-293.

[15] Standard Test Method for Microindentation Hardness of Materials. *ASTM E 384–99 (1999).*

[16] Standard Practice for Evaluating Intergranular Corrosion Resistance of Heat Treatable Aluminum Alloys by Immersion in Sodium Chloride + Hydrogen Peroxide Solution. *ASTM G110- 92(2003).*

[17] T. Luijendijk. "Welding of dissimilar aluminium alloys", *Journal of Materials Processing Technology*, Vol. 103 (2000) 29-35.

[18] H. D. Norman. "Properties of friction stir welded joints: a review of the literature"**,** AF, *EUROSTIR*, Progress report presented at the 6th PSG Meeting, 17–18 June 2003.

[19] J.M. Sánchez-Amaya, M. Bethencourt, L. González-Rovira, F.J. Botana. "Noise resistance and shot noise parameters on the study of IGC of aluminium alloys with different heat treatments", *Electrochimica Acta*, Vol. 52 (2007) 6569-6583.

Tables.

Table 1. Chemical composition of aluminium alloys (%wt).

Element	Si	Fe	Cu	Mn	Mg	Zn	Cr	Pb	Ti	Ga	V	Al
5083-T0	0.1	0.30	0.02	0.50	4.22	-	0.08	0.01	0.02	0.01	0.01	94.73
6082-T6	1.03	0.34	0.06	0.57	0.87	0.01	0.01	0.01	0.03	0.01	-	97.04

Table 2. Processing parameters of High Power Diode Laser.

Laser Beam configuration	unit	value
Emision mode	-	Continuous wave
Laser light wavelength	nm	940±10, 808±10
Laser power	W	1500 - 2750
Focus diameter	mm	2,04
Focal position	-	At specimen surface
Working distance	mm	69,3
Spot size on surface	mm^2	2,2 * 1,7
Weld bead length	mm	60

Table 3. Values of *a* and *b* of equation (1) in function of the laser source.

Alloy	Laser Source	*a* ($KJ \cdot mm^{-2}$)	*b* ($KJ \cdot mm^{-1}$)	R^2
Aluminium Alloy [6]	CO_2 laser	0.0219	0.381	0.5329
Aluminium Alloy [6]	Nd:YAG laser	0.0065	0.536	0.9801
5083 aluminium alloy	Diode Laser	0.3043	-0.647	0.9694
6082 aluminium alloy	Diode Laser	0.4900	-0.716	0.9002

Table 4. Values of *a'* and *b'* of equation (3) in function of the alloy and the laser power.

Alloy	Laser Power (KW)	*a'*	*b'* ($mm \cdot sec^{-1}$)	R^2
5083	1.5	0.3122	0.7379	0.8007
5083	2	0.3021	1.0093	0.9897
5083	2.5	0.2796	1.1699	0.9759
5083	2.75	0.2942	1.1135	0.9800
6082	2	0.3061	0.4546	0.8967
6082	2.5	0.2867	0.5365	0.9672
6082	2.75	0.2930	0.5266	0.9757
Representative values				
	a'		*b'* ($mm \cdot sec^{-1}$)	
5083	0.3		1	
6082			0.5	

Figures Captions.

Figure 1. Metallographic images of butt weld beads cross-sections of 5083 specimens, in function of the laser power and welding rate.

Figure 2. Metallographic images of butt weld beads cross-sections of 6082 specimens, in function of the laser power and welding rate.

Figure 3. Frontal view of 5083 samples totally welded (a), processed at 2 KW and 1.5 m/min and partially welded (b), processed at 1.5 KW and 3 m/min.

Figure 4. Welding efficiency of butt-welded samples of 5083 (a) and 6082 (b).

Figure 5. Depth values of butt welding beads of 5083 samples in function of the laser power and welding rate.

Figure 6. Width values of butt welding beads of 5083 samples in function of the laser power and welding rate.

Figure 7. Depth values of butt welding beads of 6082 samples in function of the laser power and welding rate.

Figure 8. Width values of butt welding beads of 6082 samples in function of the laser power and welding rate.

Figure 9. Depth*Width values of butt welding beads of 5083 and 6082 samples (double logarithmic scale) in function of the laser power and welding rate.

Figure 10. Values of $P/(v \cdot d)$ versus w^{-1} of 5083 butt welds and the fitting line to these data.

Figure 11. Values of $P/(v \cdot d)$ versus w^{-1} of 6082 butt welds and the fitting line to these data.

Figure 12. Values of d/w versus v^{-1} of 5083 butt welds.

Figure 13. Values of d/w versus v^{-1} of 6082 butt welds.

Figure 14. Real values of d and estimated values from equation 5, in function of P and v of 5082 butt welds.

Figure 15. Real values of d and estimated values from equation 6, in function of P and v of 6082 butt welds.

Figure 16. Metallographic images of cross-section of 5083 butt weld obtained at v = 1 m/min and P = 2 KW.

Figure 17. Microhardness maps of 5083 and 6082 weld beads.

Figure 18. Microhardness profiles of 5083 and 6082 weld beads.

Figure 19. Metallographic images of 5083 weld bead produced at 2 KW and 1 m/min, after the corrosion test.

Figure 20. Metallographic images of weld beads, after the corrosion test. A: 5083 at 2.5 KW and 0.5 m/min. B: 6082 at 2.5KW and 0.2 m/min.

Figure 21. Metallographic images of metal base near the weld beads, after the corrosion test. A: 5083 at 2.5 KW and 0.5 m/min. B: 6082 at 2.5KW and 0.2 m/min.

Figures

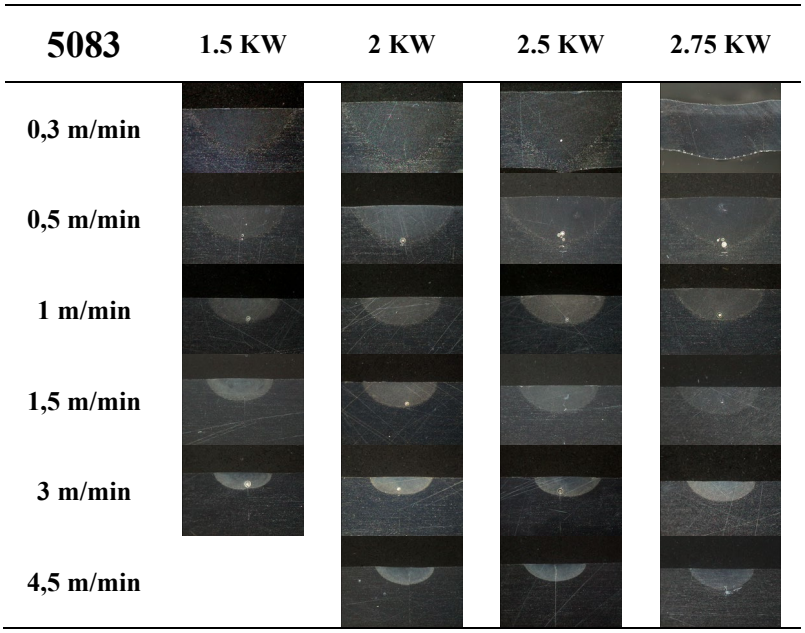

Figure 1.

6082	2 KW	2.5 KW	2.75 KW
0,2 m/min		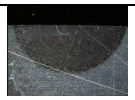	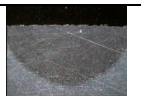
0,3 m/min			
0,5 m/min		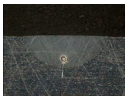	
1 m/min			
3 m/min			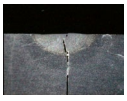
5 m/min			

Figure 2.

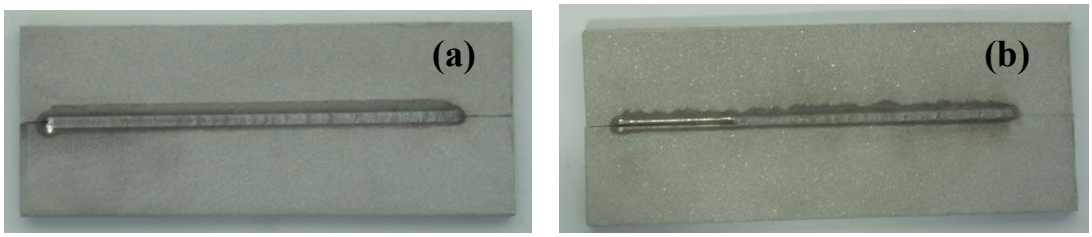

Figure 3.

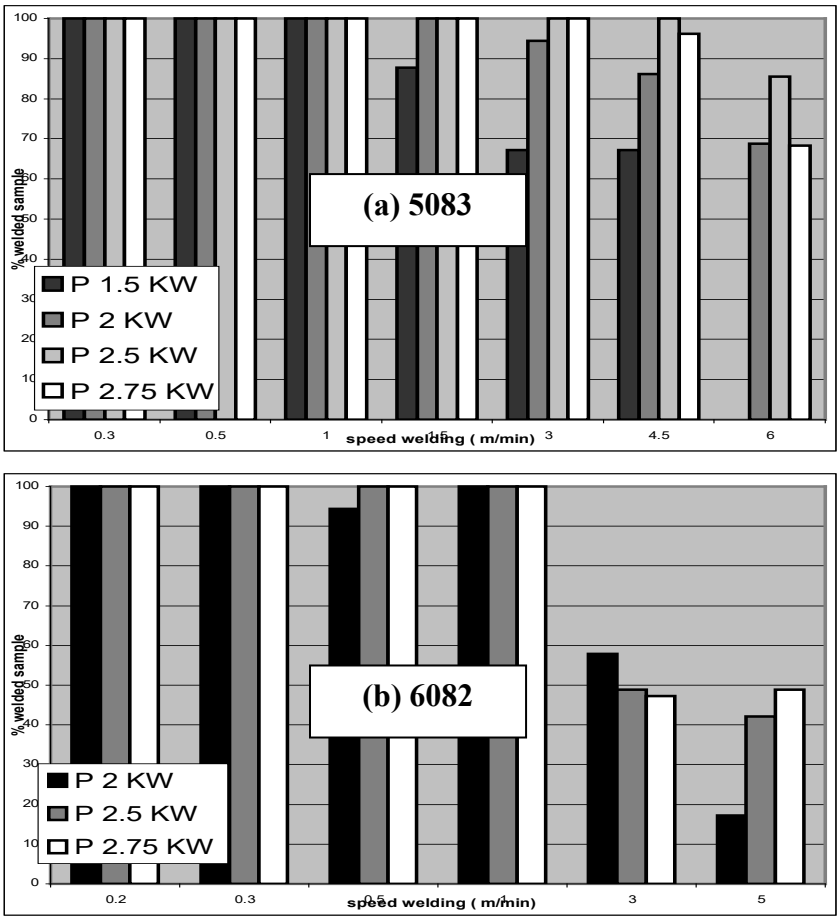
(a) 5083
% welded sample
P 1.5 KW
P 2 KW
P 2.5 KW
P 2.75 KW
speed welding (m/min)
(b) 6082
% welded sample
P 2 KW
P 2.5 KW
P 2.75 KW
speed welding (m/min)

Figure 4.

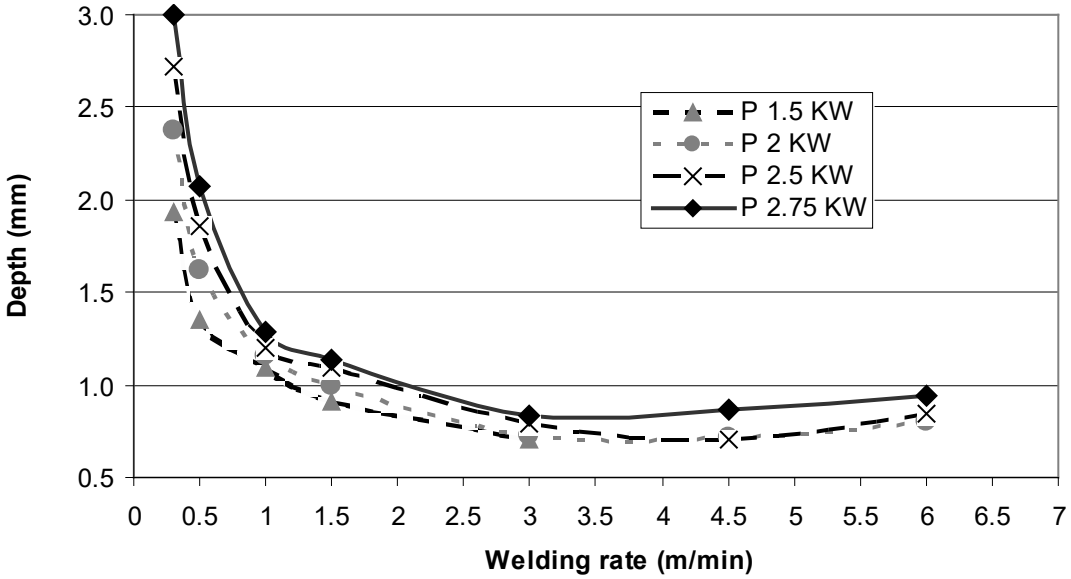
3.0
2.5
2.0
1.5
1.0
0.5
Depth (mm)
0
0.5
1
1.5
2
2.5
3
3.5
4
4.5
5
5.5
6
6.5
7
Welding rate (m/min)
P 1.5 KW
P 2 KW
P 2.5 KW
P 2.75 KW

Figure 5.

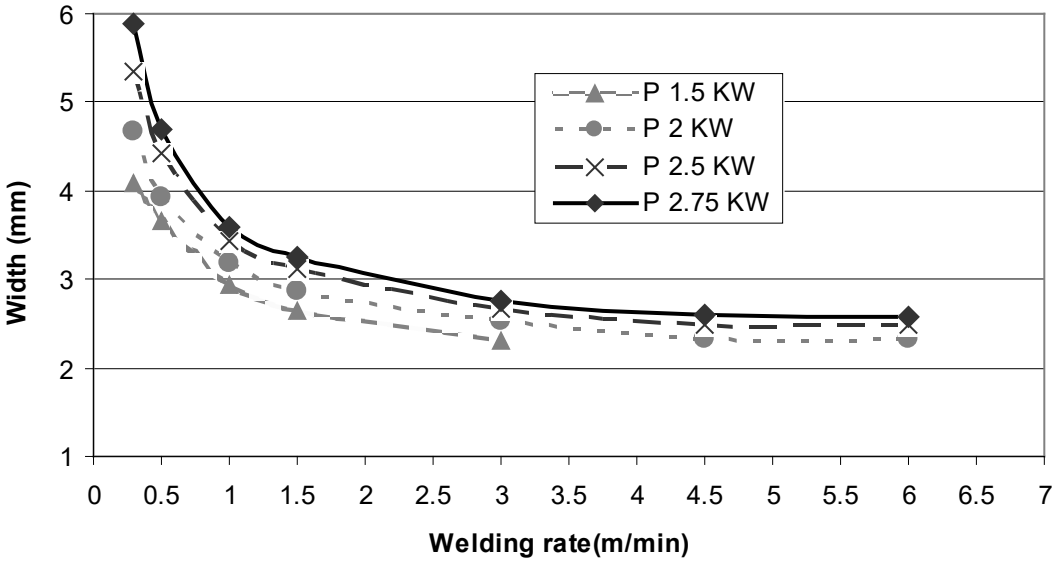
Width (mm)
Welding rate(m/min)
P 1.5 KW
P 2 KW
P 2.5 KW
P 2.75 KW
6
5
4
3
2
1
0
0.5
1
1.5
2
2.5
3
3.5
4
4.5
5
5.5
6
6.5
7

Figure 6.

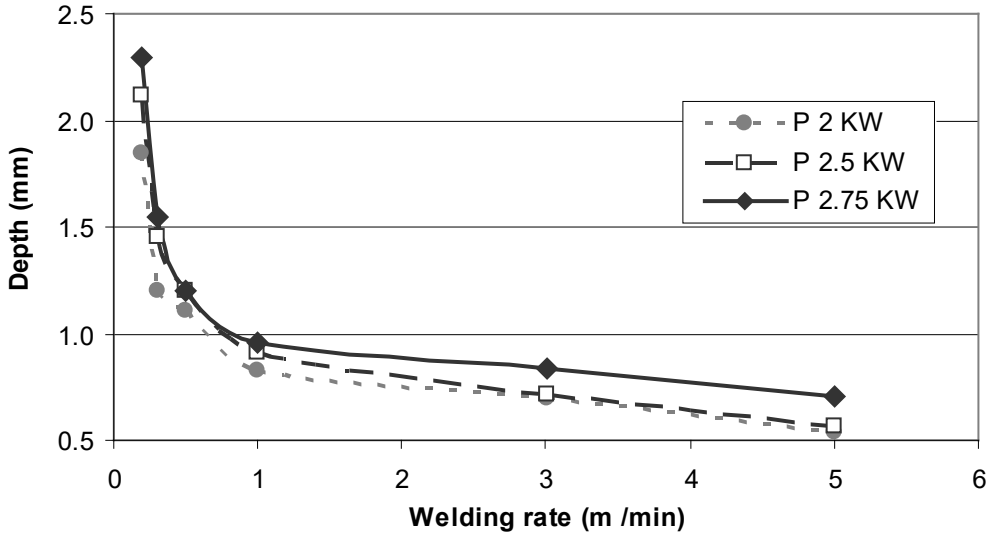
2.5
2.0
1.5
1.0
0.5
Depth (mm)
0
1
2
3
4
5
6
Welding rate (m /min)
P 2 KW
P 2.5 KW
P 2.75 KW

Figure 7.

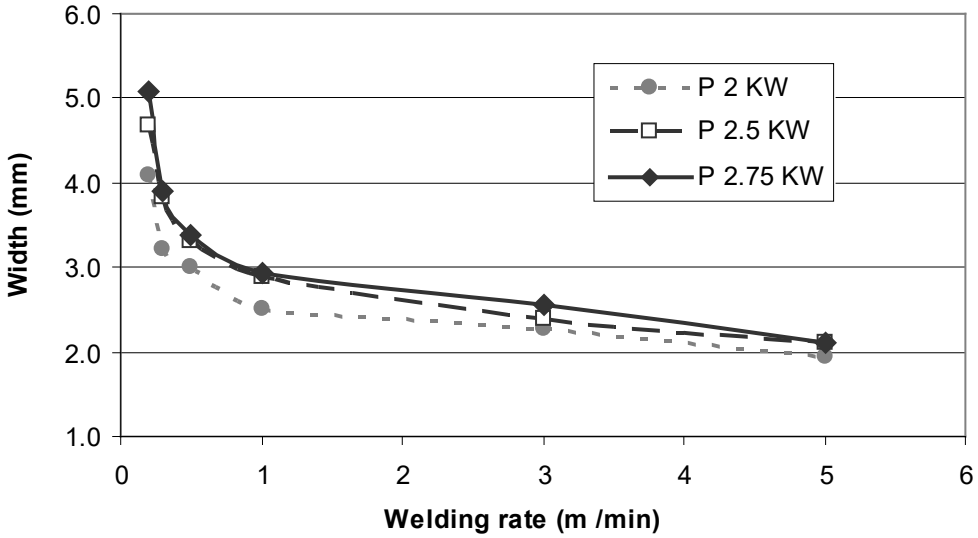
6.0
5.0
4.0
3.0
2.0
1.0
Width (mm)
0
1
2
3
4
5
6
Welding rate (m /min)
P 2 KW
P 2.5 KW
P 2.75 KW

Figure 8.

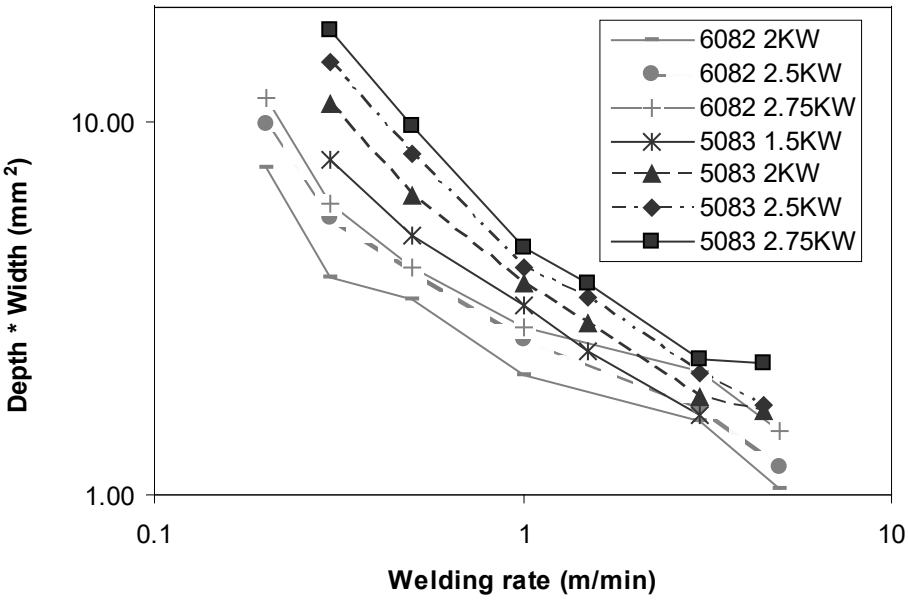
6082 2KW
6082 2.5KW
6082 2.75KW
5083 1.5KW
5083 2KW
5083 2.5KW
5083 2.75KW
10.00
1.00
0.1
1
10
Depth * Width (mm 2)
Welding rate (m/min)

Figure 9.

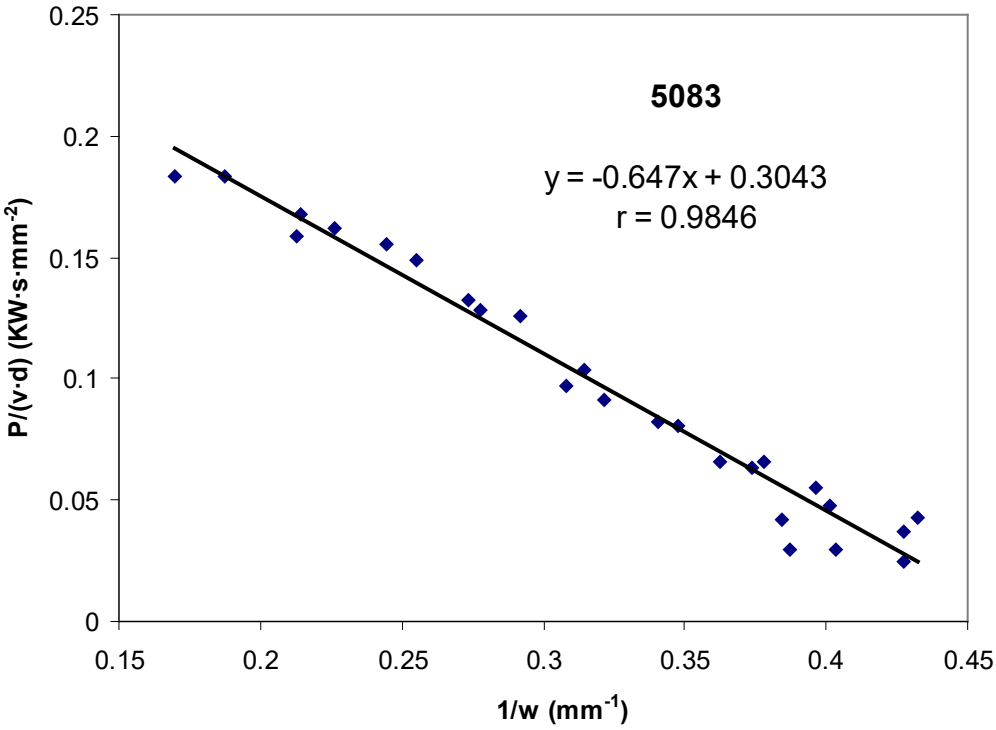
5083
y = -0.647x + 0.3043
r = 0.9846
P/(v·d) (KW·s·mm-2)
1/w (mm-1)
0.25
0.2
0.15
0.1
0.05
0
0.15
0.2
0.25
0.3
0.35
0.4
0.45

Figure 10.

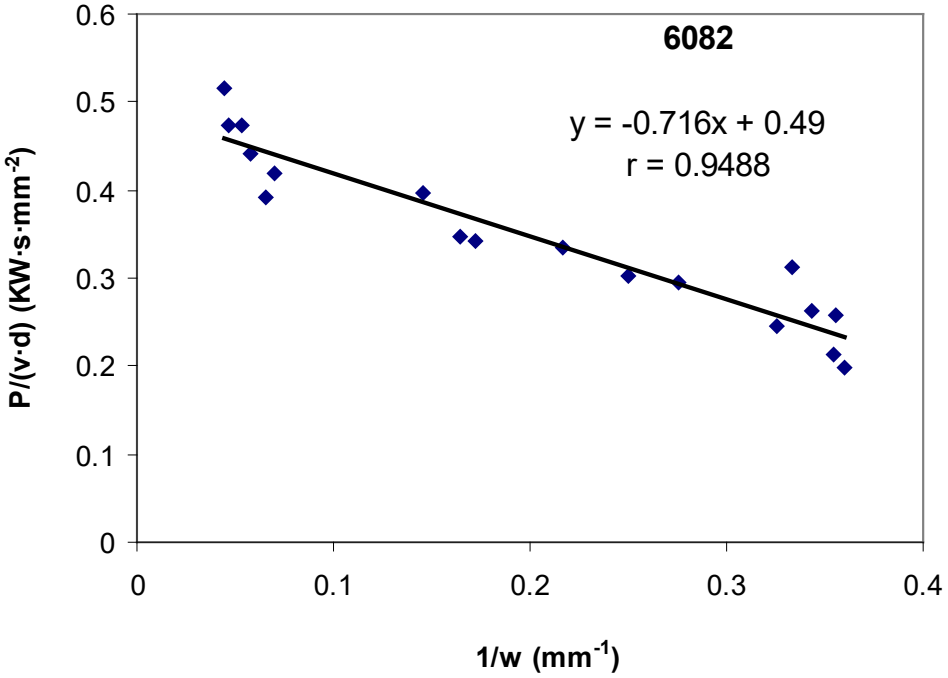
6082
y = -0.716x + 0.49
r = 0.9488
P/(v·d) (KW·s·mm-2)
1/w (mm-1)
0.6
0.5
0.4
0.3
0.2
0.1
0
0
0.1
0.2
0.3
0.4

Figure 11.

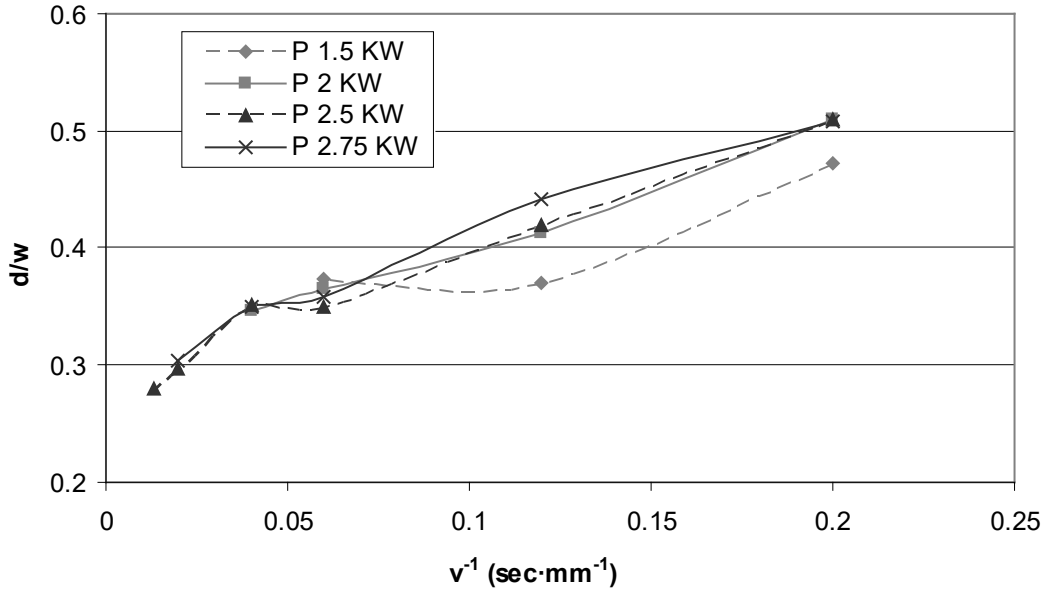
0.6
0.5
0.4
0.3
0.2
d/w
P 1.5 KW
P 2 KW
P 2.5 KW
P 2.75 KW
0
0.05
0.1
0.15
0.2
0.25
v-1 (sec·mm-1)

Figure 12.

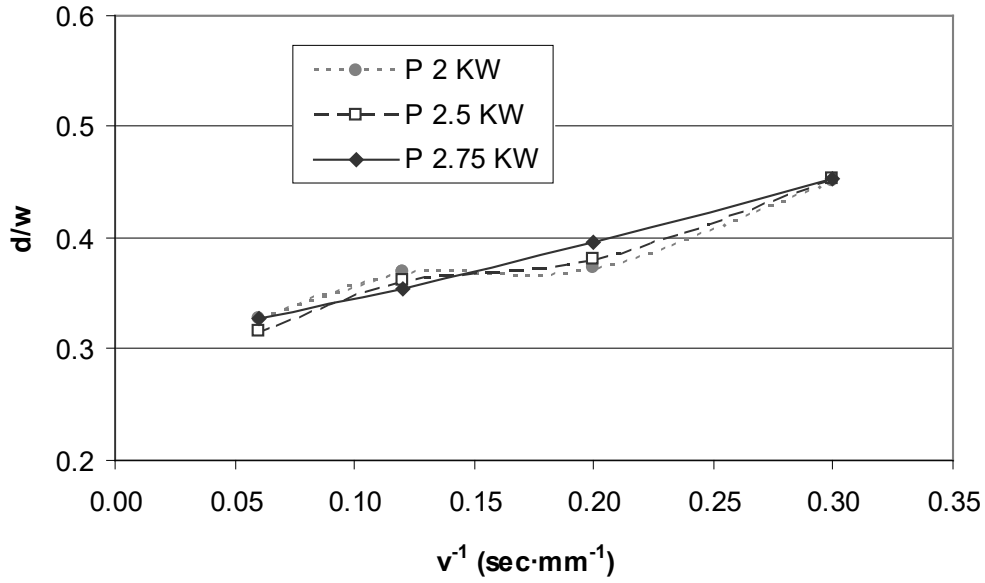
0.6
0.5
0.4
0.3
0.2
d/w
P 2 KW
P 2.5 KW
P 2.75 KW
0.00
0.05
0.10
0.15
0.20
0.25
0.30
0.35
v-1 (sec·mm-1)

Figure 13.

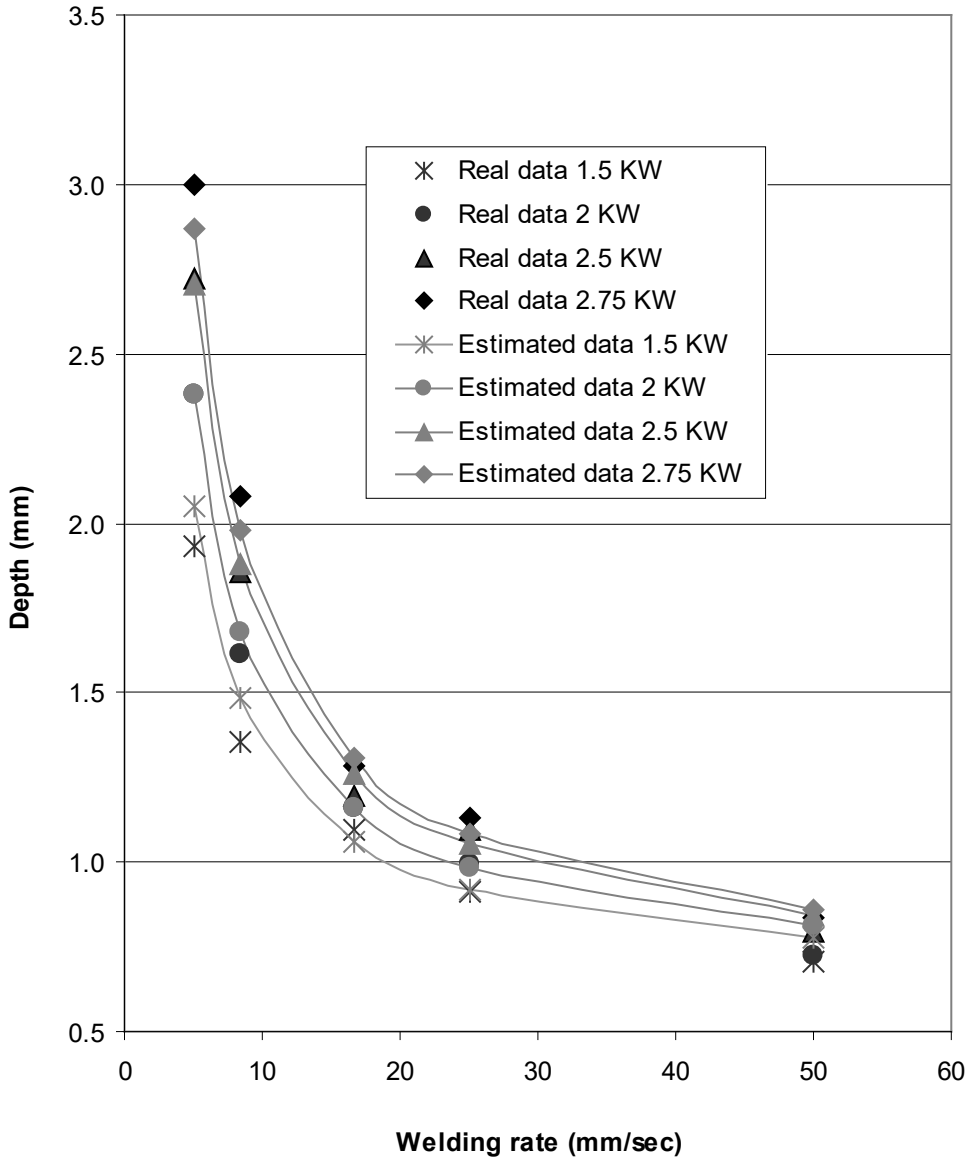
3.5
3.0
2.5
2.0
1.5
1.0
0.5
Depth (mm)
0
10
20
30
40
50
60
Welding rate (mm/sec)
Real data 1.5 KW
Real data 2 KW
Real data 2.5 KW
Real data 2.75 KW
Estimated data 1.5 KW
Estimated data 2 KW
Estimated data 2.5 KW
Estimated data 2.75 KW

Figure 14.

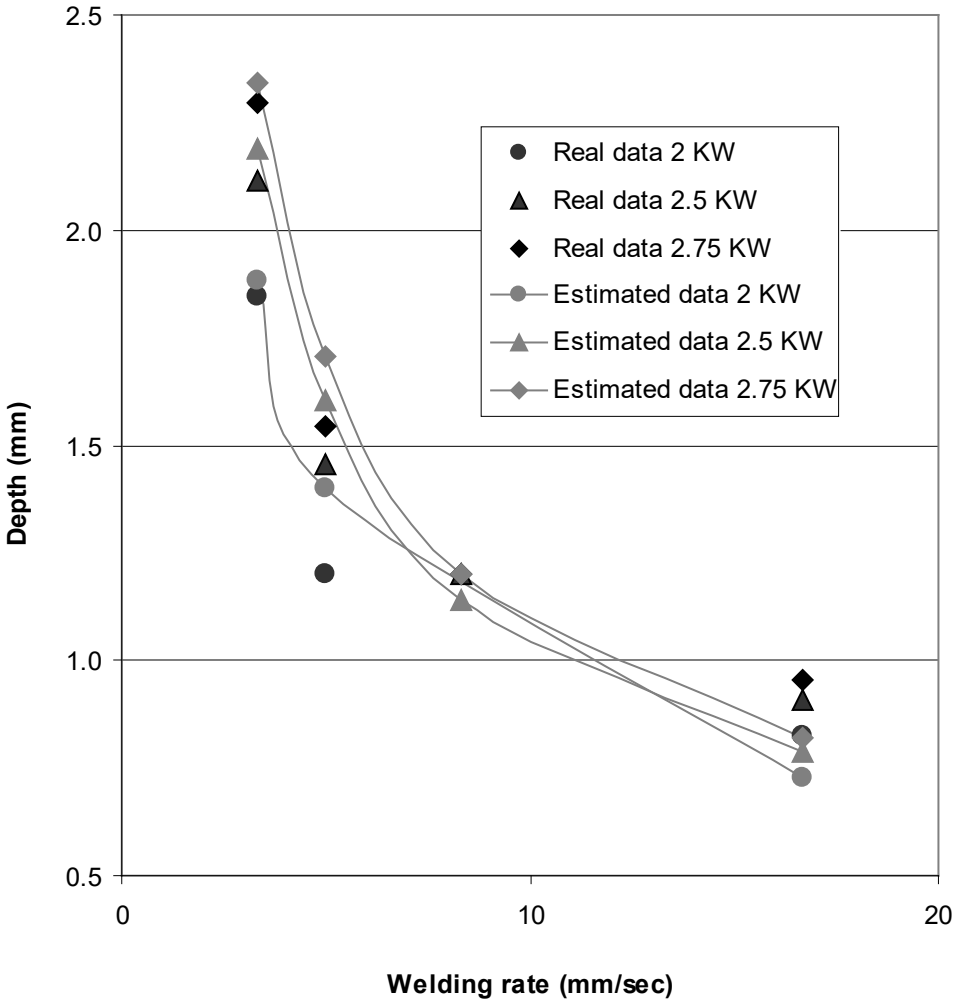
2.5
2.0
1.5
1.0
0.5
Depth (mm)
0
10
20
Welding rate (mm/sec)
Real data 2 KW
Real data 2.5 KW
Real data 2.75 KW
Estimated data 2 KW
Estimated data 2.5 KW
Estimated data 2.75 KW

Figure 15.

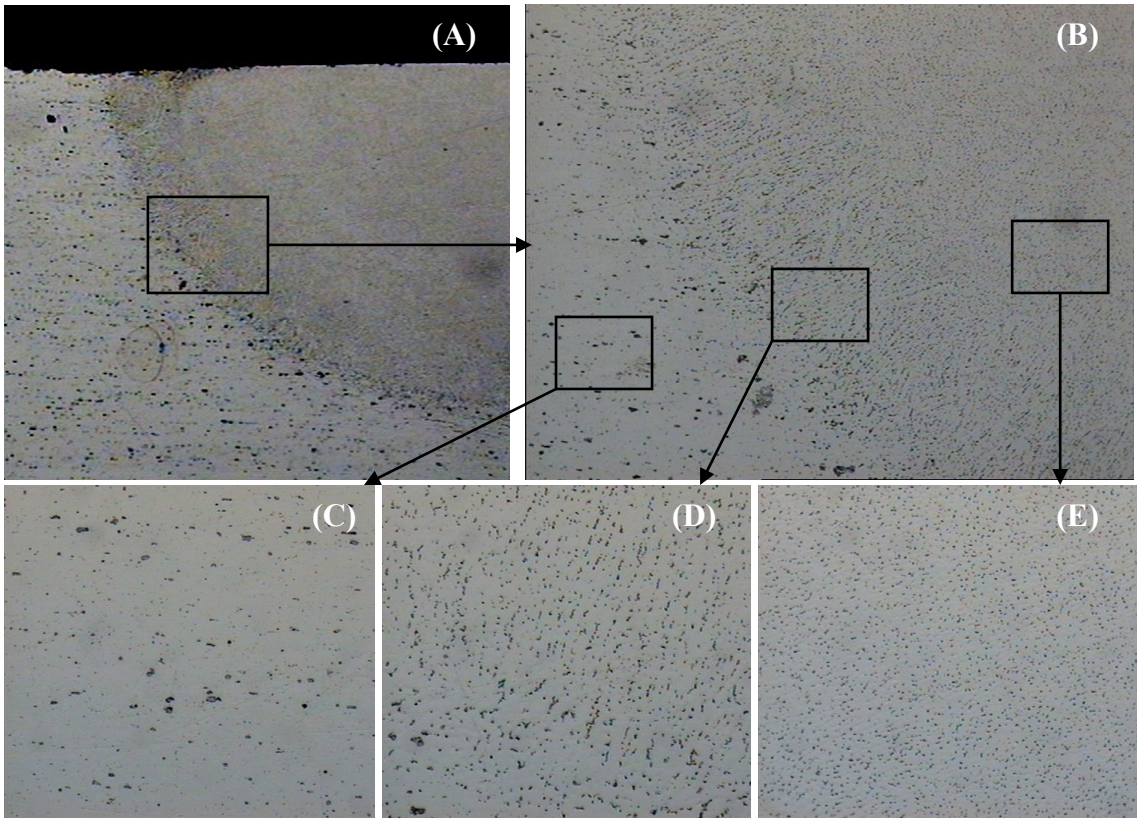

Figure 16.

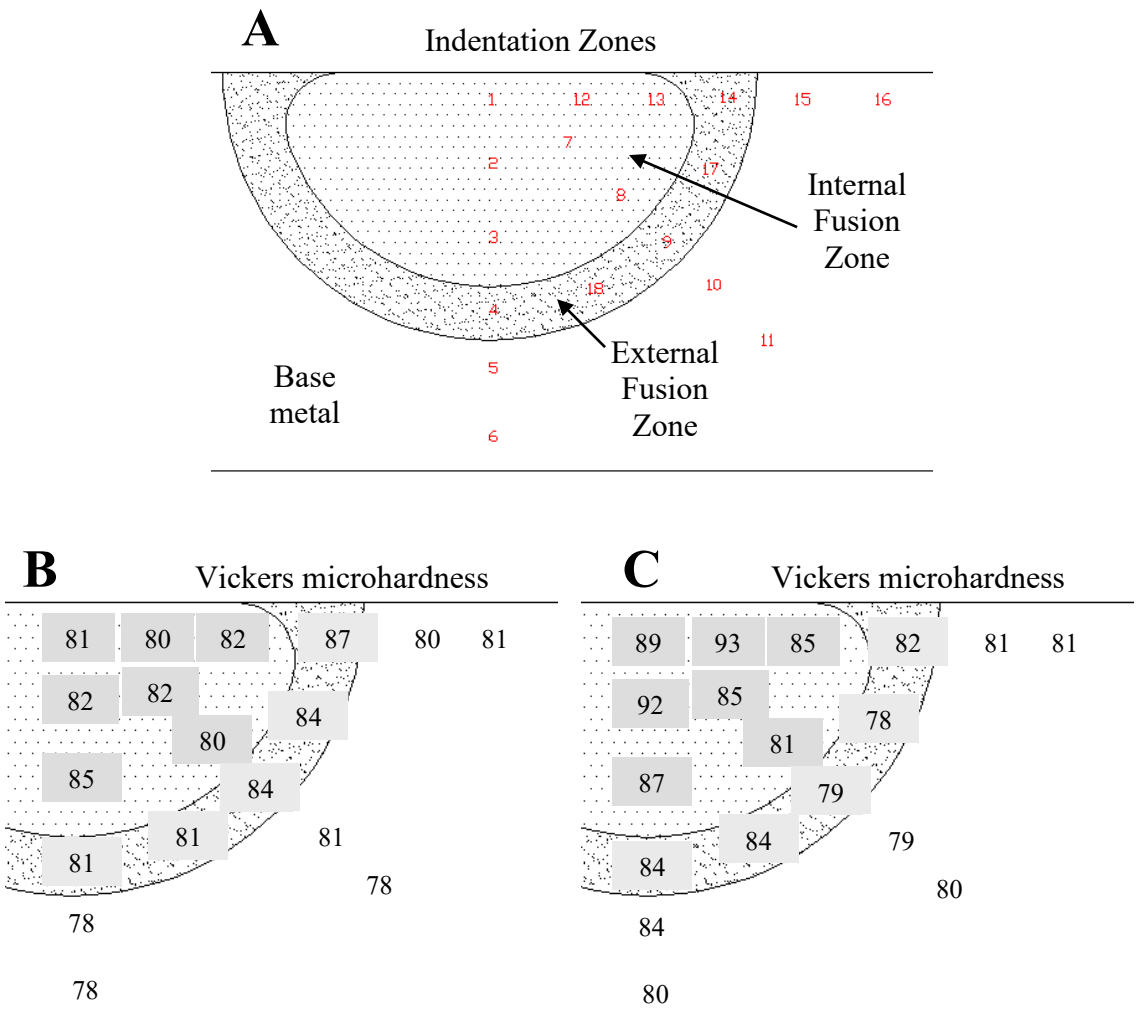
A
Indentation Zones
1
12
13
14
15
16
7
2
17
8
3
9
10
18
4
11
5
6
Internal
Fusion
Zone
External
Fusion
Zone
Base
metal
B
Vickers microhardness
81
80
82
87
80
81
82
82
84
80
85
84
81
81
81
78
78
78
C
Vickers microhardness
89
93
85
82
81
81
92
85
78
81
87
79
84
79
84
80
84
80

Figure 17.

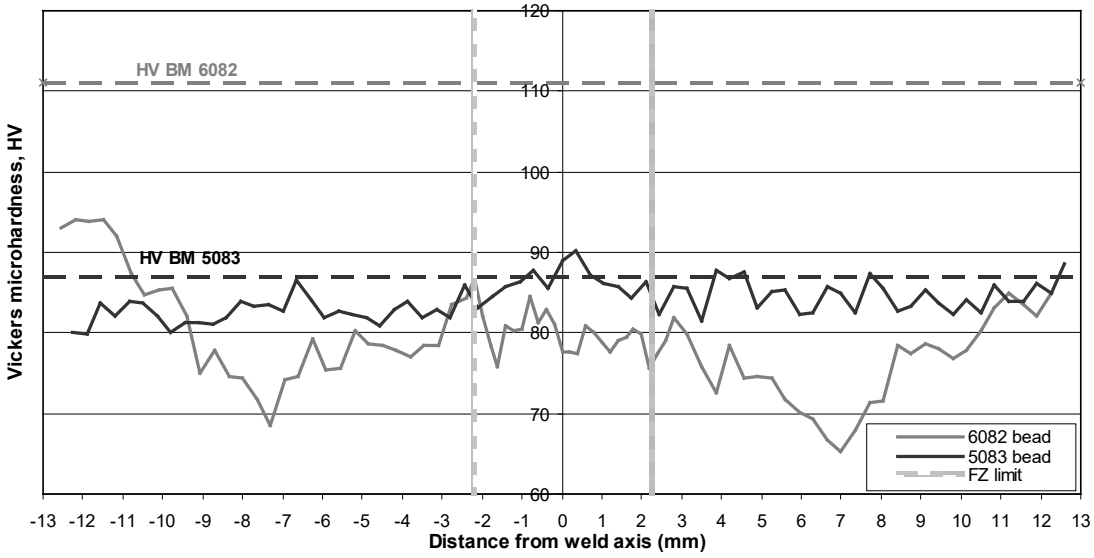
HV BM 6082
HV BM 5083
Vickers microhardness, HV
120
110
100
90
80
70
60
-13 -12 -11 -10 -9 -8 -7 -6 -5 -4 -3 -2 -1 0 1 2 3 4 5 6 7 8 9 10 11 12 13
Distance from weld axis (mm)
6082 bead
5083 bead
FZ limit

Figure 18.

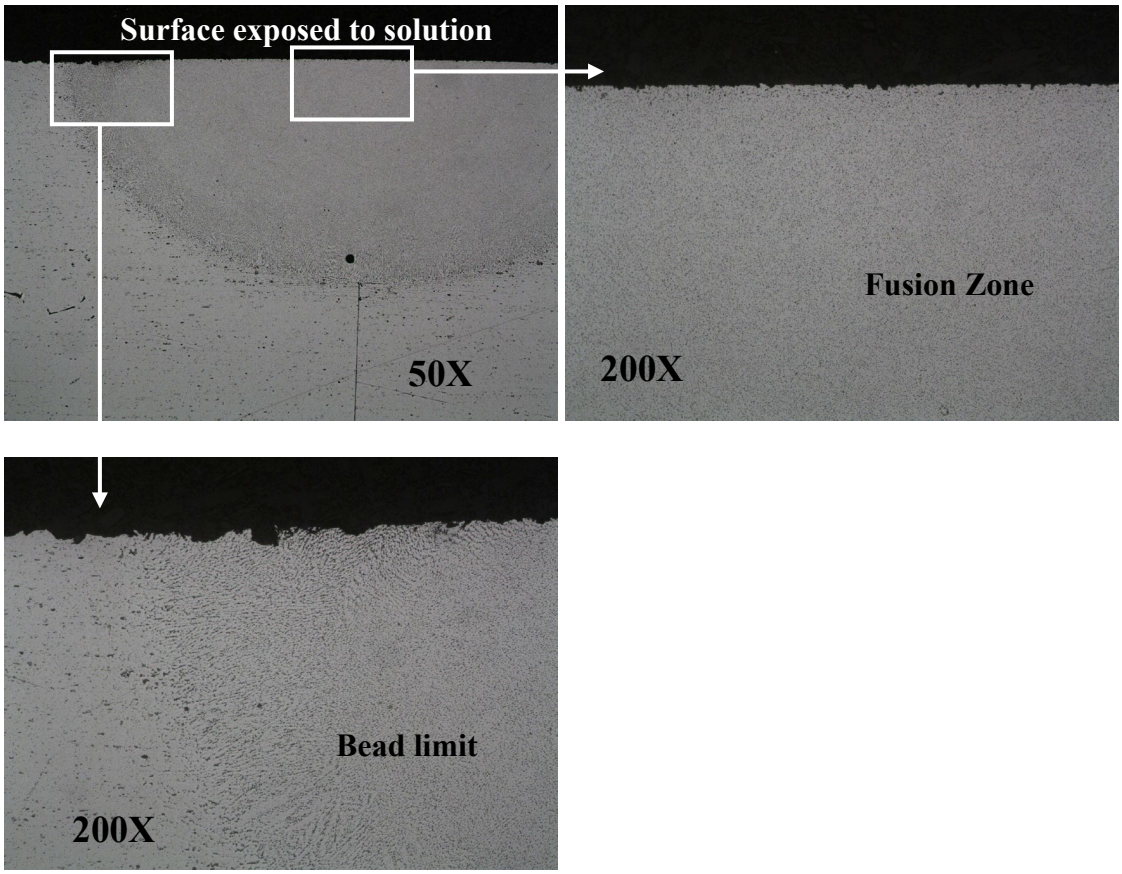
Surface exposed to solution
50X
Fusion Zone
200X
Bead limit
200X

Figure 19.

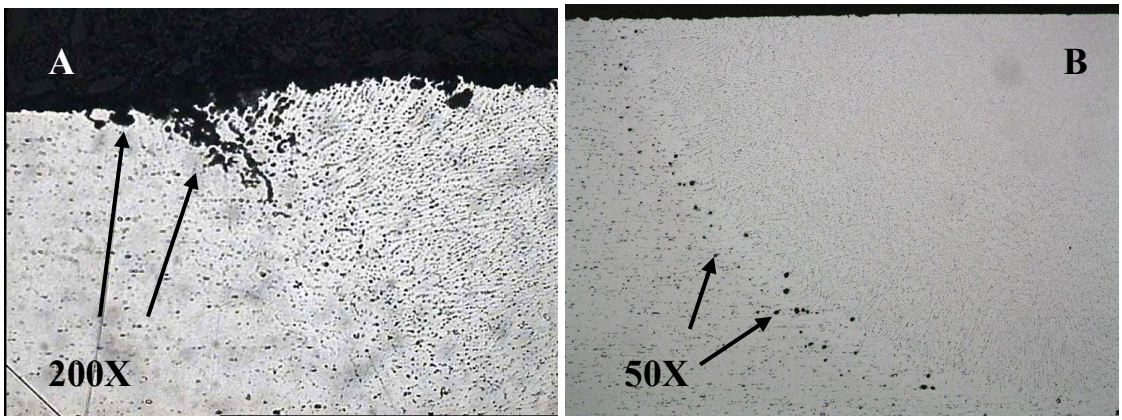

Figure 20.

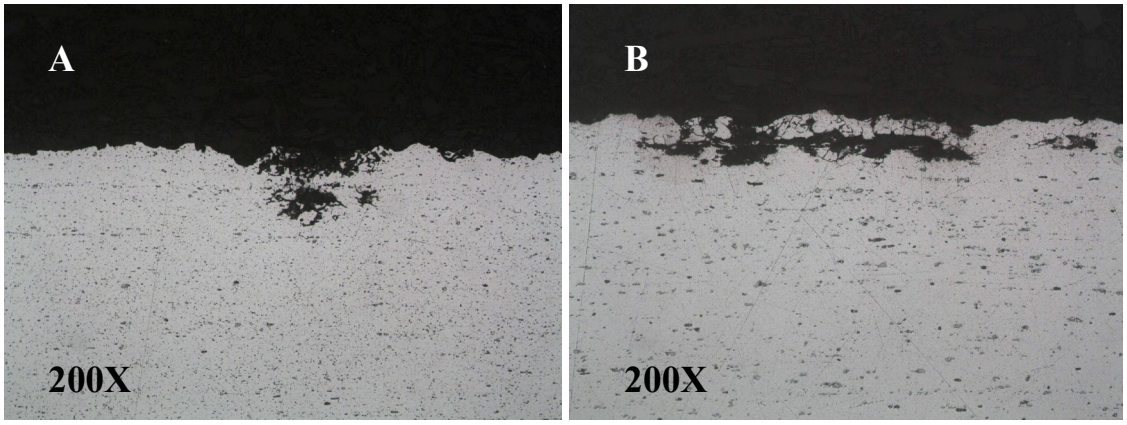

Figure 21.